



Title	Water partitioning in the Earth's mantle
Author(s)	Inoue, Toru; Wada, Tomoyuki; Sasaki, Rumi; Yurimoto, Hisayoshi
Citation	Physics of the Earth and Planetary Interiors, 183(1-2), 245-251 https://doi.org/10.1016/j.pepi.2010.08.003
Issue Date	2010-11
Doc URL	http://hdl.handle.net/2115/44920
Type	article (author version)
File Information	PEPI183-1-2_245-251.pdf



[Instructions for use](#)

Water partitioning in the Earth's mantle

Toru Inoue¹, Tomoyuki Wada¹, Rumi Sasaki¹, Hisayoshi Yurimoto²

¹Geodynamics Research Center, Ehime University, Bunkyo-cho 2-5,
Matsuyama, Ehime 790-8577, Japan

²Division of Earth and Planetary Sciences, Hokkaido University,
Sapporo 060-0810, Japan

Physics of the Earth and Planetary Interiors 183 (2010) 245-251

Abstract We have conducted H₂O partitioning experiments between wadsleyite and ringwoodite and between ringwoodite and perovskite at 1673K and 1873K, respectively. These experiments were performed in order to constrain the relative distribution of H₂O in the upper mantle, the mantle transition zone, and the lower mantle. We successfully synthesized coexisting mineral assemblages of wadsleyite-ringwoodite and ringwoodite-perovskite that were large enough to measure the H₂O contents by secondary ion mass spectrometry (SIMS). Combining our previous H₂O partitioning data (Chen et al., 2002) with the present results, the determined water partitioning between olivine, wadsleyite, ringwoodite, and perovskite under H₂O-rich fluid saturated conditions are 6: 30: 15 : 1, respectively. Because the maximum H₂O storage capacity in wadsleyite is ~3.3 wt% (e.g. Inoue et al, 1995), the possible maximum H₂O storage capacity in the olivine high pressure polymorphs are as follows: ~0.7 wt% in olivine (upper mantle just above 410 km depth), ~3.3 wt% in wadsleyite (410-520 km depth), ~1.7 wt% in ringwoodite (520-660 km depth), and ~0.1 wt% in perovskite (lower mantle). If we assume ~0.2 wt% of the H₂O content in wadsleyite in the mantle transition zone estimated by recent electrical conductivity measurements (e.g. Dai and Karato, 2009), the estimated H₂O contents throughout the mantle are as follows; ~0.04 wt% in olivine (upper mantle just above 410 km depth), ~0.2 wt% in wadsleyite (410-520 km depth), ~0.1 wt% in ringwoodite (520-660 km depth) and ~0.007 wt% in perovskite (lower mantle). Thus, the mantle transition zone should contain a large water reservoir in the Earth's mantle compared to the upper mantle and the lower mantle.

34 Key words: mantle, olivine, wadsleyite, ringwoodite, perovskite, hydrous wadsleyite,
35 hydrous ringwoodite, high pressure phase transformation, partitioning of H₂O

36

37 **1. Introduction**

38 Water, the most abundant volatile component on the Earth's surface, has been
39 supplied to the Earth's mantle by subducting slabs from the lithosphere (e.g. Irifune et
40 al.,1998; Ohtani et al., 2004). Because water influences the physical properties and
41 melting temperature of minerals, it is important to constrain the potential amount of
42 water in nominally anhydrous phases at various depths in the Earth's mantle.

43 Olivine (α -phase) and the high pressure polymorphs of olivine are the most abundant
44 minerals in the upper mantle, and the high-pressure polymorphs of olivine, wadsleyite
45 (β -phase), and ringwoodite (γ -phase), can contain up to 2-3 wt% of H₂O in their crystal
46 structures (e.g. Inoue et al., 1995, 1998; Kohlstedt et al., 1996). However, the
47 partitioning data of H₂O between these minerals are few except for the
48 olivine-wadsleyite transformation (Chen et al., 2002) and ringwoodite-perovskite
49 transformation (Bolfan-Casanova et al., 2003). We have determined the partitioning of
50 H₂O between wadsleyite and ringwoodite and between ringwoodite and perovskite at
51 1673K and 1873K, respectively. These temperatures are close to typical mantle
52 temperature proposed by Brown and Shankland (1981) and Katsura et al. (2009) at the
53 520 km and 660 km seismic discontinuity. We have also ascertained the relative
54 distribution of H₂O among the upper mantle, the mantle transition zone, and the lower
55 mantle.

56

57 **2. Experimental**

58 High-pressure experiments were conducted in an MA-8 type (Kawai-type)
59 high-pressure apparatus at Ehime University. The truncation edge lengths (TEL) of the
60 cubic anvils were 3.5 and 2.5 mm for the experiments on wadsleyite-ringwoodite and
61 ringwoodite-perovskite, respectively. We used semi-sintered magnesia that was doped
62 with 17 wt % CoO and LaCrO₃ as the pressure medium, and ZrO₂ was used as the
63 thermal insulator. We adopted a cylindrical platinum (Pt) or rhenium (Re) heater with a
64 wall thickness of ~30 μ m. The typical cell assembly used with TEL of 3.5 mm is shown
65 in Fig. 1.

66 The starting materials were a mixture of Mg(OH)₂, Fe₂SiO₄ and SiO₂ reagent with the

67 chemical composition of $(\text{Mg}_{0.8}\text{Fe}_{0.2})_2\text{SiO}_4$ plus 15.8 wt% H_2O (Table 1). Thus, H_2O
68 was introduced by $\text{Mg}(\text{OH})_2$, and ferrous iron was introduced by Fe_2SiO_4 because
69 wustite (Fe_{1-x}O) is non-stoichiometric. The reason we selected such large water content
70 was to enhance the crystal growth and to make it possible to measure the H_2O content
71 precisely by secondary ion mass spectroscopy (SIMS). In addition, the reason we
72 selected the olivine composition of $(\text{Mg}_{0.8}\text{Fe}_{0.2})_2\text{SiO}_4$ was to enhance the coexisting
73 region of wadsleyite-ringwoodite and ringwoodite-perovskite in order to obtain the
74 sample.

75 A corresponding anhydrous starting material was also prepared. The appropriate
76 mechanical mixture of Mg_2SiO_4 and Fe_2SiO_4 powders was used for the composition of
77 $(\text{Mg}_{0.8}\text{Fe}_{0.2})_2\text{SiO}_4$. Both anhydrous and hydrous samples were enclosed in a welded
78 $\text{Au}_{75\%}\text{Pd}_{25\%}$ alloy capsule separately before loading into a high pressure cell in order to
79 avoid the loss of both water and iron. Platinum is often used as capsule material, but it
80 absorbs iron significantly. Therefore, we used $\text{Au}_{75\%}\text{Pd}_{25\%}$ to make the loss of Fe less,
81 which is superior to Pt in an iron bearing system, as the capsule material.

82 Temperature was measured with a W_{97}Re_3 - $\text{W}_{75}\text{Re}_{25}$ thermocouple junction placed in
83 the center of the furnace assembly. The fluctuation of temperature throughout the run
84 was kept within $\pm 5^\circ\text{C}$ in each condition, but no pressure correction was made for the
85 emf of the thermocouple.

86 Careful pressure calibration was done on the basis of the present anhydrous
87 experiments of the wadsleyite-ringwoodite phase transition based on the
88 thermochemical phase diagram (Akaogi et al., 1989) at 1673K, and the postspinel phase
89 transition (Ito and Takahashi, 1989) at 1873K. Therefore, the pressure conditions for
90 the coexisting run products wadsleyite-ringwoodite and ringwoodite-perovskite were
91 determined by fitting our anhydrous compositional data on the loop by Akaogi et
92 al.(1989) and Ito and Takahashi (1989). In this case, the relative pressure precision in
93 the runs with the coexisting wadsleyite-ringwoodite and coexisting
94 ringwoodite-perovskite under anhydrous conditions is estimated to be about 0.05 GPa,
95 and about 0.2 GPa in runs without co-existing phases.

96 In high-pressure and high-temperature experiments, pressure was applied first to the
97 target ram loads, then the temperature was kept constant for 20-120 minutes before
98 quenching by turning off power to the furnace, and then the run was quenched by

99 turning off the electric power. The recovered charges were polished for phase
100 identification and chemical analysis.

101 The phases were identified by a micro-focused X-ray diffractometer and by
102 micro-Raman spectroscopy. The chemical compositions were determined by EPMA and
103 the water content of the minerals was measured by SIMS at Hokkaido University.

104 The SIMS instrument used in the present study was the Cameca IMS-3F ion mass
105 microanalyzer. The polished samples were coated with a gold film 300 Å in thickness
106 for SIMS analysis. A primary beam operated at ~10 nA, 12.5 kV $^{16}\text{O}^-$ was focused to
107 form an ~30 μm spot on the sample, and the secondary $^1\text{H}^+$ and $^{30}\text{Si}^+$ ions were
108 collected from the center region (10 μm in diameter) of the sputtered area using a
109 mechanical aperture to minimize artifacts arising from hydrogen adsorption on the
110 polished sample surface. The H_2O content of samples was calibrated from relative
111 intensities of $^1\text{H}^+ / ^{30}\text{Si}^+$ using an empirical linear relationship (Yurimoto et al., 1989). We
112 used natural amphibole crystal with a water content of 1.66 wt % for a standard, which
113 was determined by a hydrogen gas manometry method with the accuracy of ± 0.1 wt%
114 (Miyagi and Yurimoto, 1995). In addition, San Carlos olivine was used for the
115 background H intensities, because the H concentration is considerably small (10-60
116 ppm: Kurosawa et al. 1997), compared with the present H concentration in our samples.

117 We obtained a depth profile of the intensity of $^1\text{H}^+$ and $^{30}\text{Si}^+$ with time. The
118 steady-state hydrogen emission achieved depends on the H concentration, but usually it
119 is achieved after 30-60 minute bombardments of the primary ions with H_2O
120 concentration of ~1 wt%. The uncertainty of the H_2O content in the present analysis is ~
121 $\pm 10\%$, which mainly comes from the scattering of the measured $^1\text{H}^+ / ^{30}\text{Si}^+$ value for
122 several standard measurements, probably because of the slightly chemical heterogeneity
123 of the present natural amphibole standard. More details for the SIMS measurement are
124 described in Miyagi and Yurimoto (1995), and the water content and the chemical
125 composition of the present amphibole standard was shown in Table 1 (ICH) of Miyagi
126 et al. (1998).

127

128 **3. Results and discussion**

129 The experimental conditions and results are summarized in Tables 2 and 3. The
130 experiments were conducted at conditions of 14.6-17.0 GPa and 1673K for the
131 wadsleyite-ringwoodite experiment and ~23 GPa and 1873K for the

132 ringwoodite-perovskite experiments. The heating durations were 20-120 minutes.

133 All experiments were performed under H₂O-rich fluid (melt) saturated conditions
134 where solid phases coexisted with a hydrous melt, as evidenced by fibrous crystals and
135 spinifex texture in the quench product. These results show the formation of liquid under
136 all conditions.

137 Note that at the present experimental conditions in the silicate-H₂O system,
138 H₂O-bearing silicate melt (liquid) and H₂O-rich aqueous fluid cannot be distinguished
139 from each other because of the existence of the second critical end point (e.g. Mibe et
140 al., 2007). So the terminology of melt (liquid) and fluid in this paper has the same
141 meaning.

142

143 **3-1. The effect of water on the phase boundary between wadsleyite and** 144 **ringwoodite**

145 We observed the coexistence of wadsleyite and ringwoodite at pressures of 15.6 to
146 16.5 GPa under anhydrous conditions, whereas the coexistence of both wadsleyite and
147 ringwoodite were not observed below 16.4 GPa under hydrous conditions (Table 2).
148 This shows that the phase boundary between wadsleyite and ringwoodite moves to
149 higher pressure under water-bearing conditions.

150 Table 4 shows the Fe/(Mg+Fe) in wadsleyite and ringwoodite and the corresponding
151 partition coefficient at each pressure. We define the partition coefficient, K_d, as
152 $(\text{Fe}/\text{Mg})_{\gamma}/(\text{Fe}/\text{Mg})_{\beta}$. The K_ds were ~1.6-1.7 in both the anhydrous and hydrous systems,
153 which are consistent with our previous report (Inoue et al, 2010).

154 Figures 2(a) and 2(b) show the high pressure phase diagrams of wadsleyite and
155 ringwoodite in the Mg₂SiO₄-Fe₂SiO₄ system under anhydrous and hydrous conditions,
156 respectively, by using the present Fe/(Mg+Fe) data for wadsleyite and ringwoodite.

157 At 15.6 GPa (Run E1766), the coexistence of wadsleyite and ringwoodite starts to
158 appear in the anhydrous system, but ringwoodite does not appear in the hydrous system.
159 This trend for the anhydrous and hydrous systems continues up to 16.5 GPa (Run
160 E1794), and the coexistence of wadsleyite and ringwoodite appears at 16.5 GPa (Run
161 E1760, E1751) in the hydrous system. In run E1788 (P≈17 GPa), only ringwoodite
162 was observed under anhydrous conditions, but the coexistence of wadsleyite and
163 ringwoodite was still observed under hydrous conditions.

164 This result indicates that the loop of the wadsleyite and ringwoodite boundary shifts
165 towards higher pressure or higher iron content, and the pressure width of the loop
166 decreased with the effect of H₂O. The present observation is consistent with our
167 previous result of 1 wt% H₂O (Inoue et al., 2010).

168 We have already determined that the phase boundary between olivine and wadsleyite
169 shifts to lower pressures under water bearing conditions (Chen et al., 2002; Inoue et al.,
170 2009). Combining the present results with our previous data, it is clear that the stability
171 region of wadsleyite expands and the pressure width of the divariant loop decreases for
172 both of the phase boundaries between olivine and wadsleyite, and between wadsleyite
173 and ringwoodite.

174 In the present study, the experiments were performed under H₂O-rich fluid saturated
175 conditions, so note that the width of the loop can only be applied to H₂O-rich fluid
176 saturated conditions, and the width of the loop should be narrower than those in
177 H₂O-rich fluid undersaturated conditions when considering the phase diagram of the
178 pure-Mg system (Frost and Dolejs, 2007). However, the important point is that the
179 amounts of Mg and Fe in the coexisting phases are different between anhydrous and
180 hydrous conditions (Inoue et al.2010). The present results reflect the system with
181 Mg-Fe partitioning under H₂O-rich fluid saturated condition.

182 For the hydrous melting phase relation, clinoenstatite was observed in the liquidus
183 phase below ~17 GPa, and then changed to stishovite. These results indicate that
184 MgO-rich (ultrabasic) liquid was formed under hydrous melting conditions, which are
185 consistent with our previous results (Inoue at al., 1994; Yamada et al., 2004).

186

187 **3-2. The effect of water on postspinel phase boundary**

188 The coexisting region of ringwoodite and perovskite was quite narrow in both the
189 anhydrous and hydrous systems, so it was difficult to determine the exact loop in this
190 boundary. However, we could observe the coexistence of ringwoodite and perovskite at
191 pressures of 23.0-23.2 GPa (runs E1784, E1730 and E1695).

192 At 23.0 GPa (E1784), the Fe/(Mg+Fe) ratios in ringwoodite, perovskite, and
193 magnesiowustite were 0.199, 0.086 and 0.342, respectively, whereas in the hydrous
194 system, the Fe/(Mg+Fe) ratios in ringwoodite and perovskite were 0.159 and 0.056,
195 respectively. We could not observe magnesiowustite in the most hydrous run, because
196 the composition of the hydrous liquid became MgO rich with increasing pressure, as we

197 have already reported (Inoue, 1994; Yamada et al., 2004), and magnesiowustite tends to
198 dissolve in the liquid. The reason why the Fe/(Mg+Fe) ratios of ringwoodite and
199 perovskite in the hydrous system is much lower than those in anhydrous conditions is
200 the existence of the hydrous liquid. The hydrous liquid prefers iron compared to
201 crystalline phases. Nevertheless, the partition coefficients, $K_d = (\text{Fe}/\text{Mg})_{\text{Pv}}/(\text{Fe}/\text{Mg})_{\text{r}}$,
202 were almost the same ($\sim 0.3\sim 0.4$) in both anhydrous and hydrous systems.

203 We have already reported the effect of water on the spinel-postspinel transformation
204 in Mg_2SiO_4 , and reported that the boundary moves to high pressures by ~ 0.2 GPa under
205 water bearing conditions, compared with anhydrous conditions (Higo et al., 2001). In
206 the present experiment, we could not observe the phenomena clearly because of the
207 fluctuation of the generated pressure in each cell assembly. In the hydrous system this
208 was also caused by the complicated phase assembly in each run. Nevertheless, the main
209 purpose of the present experiment was to obtain the coexisting sample of ringwoodite
210 and perovskite to determine the H_2O content and the partitioning effect. We succeeded
211 in this purpose, which will be further described later.

212

213 **3-3. The H_2O content and partitioning in wadsleyite, ringwoodite and** 214 **perovskite**

215 We succeeded in synthesizing large ($\sim 50\mu\text{m}$) crystals of coexisting wadsleyite and
216 ringwoodite, and of ringwoodite and perovskite. Figures 3 and 4 show the back
217 scattered electron images of the coexisting run products of wadsleyite and ringwoodite
218 (E1751, E1760), and of ringwoodite and perovskite (E1748 and E1730), respectively. In
219 all run products, hydrous liquids coexisted with the minerals. In addition, clinoenstatite
220 existed in the liquidus phase at ~ 16.5 GPa and 1673K under hydrous melting
221 conditions.

222 Table 6 shows the H_2O contents in wadsleyite and ringwoodite at ~ 16.5 GPa and
223 1673K, and the corresponding partition coefficient. The H_2O contents in wadsleyite and
224 ringwoodite at ~ 16.5 GPa and 1673K were 1.8-2.3 wt% and 1-1.25 wt%, respectively.
225 In E1788, the H_2O content was higher than that in the other runs, because the
226 temperature was estimated by the power supply and the generated temperature may
227 have been lower than 1673K. For this reason, the amount of hydrous melt was small and
228 the H_2O contents in the crystals became higher in E1788. In spite of this difference, the
229 partition coefficient between wadsleyite and ringwoodite ($K_d = (\text{H}_2\text{O})_{\beta}/(\text{H}_2\text{O})_{\gamma}$) was ~ 2 ;

230 this result shows that wadsleyite favors H₂O twice as much when compared to
231 ringwoodite.

232 Table 7 shows the H₂O content in ringwoodite and perovskite at ~23 GPa and 1873K,
233 and the partition coefficient. The H₂O content in ringwoodite and perovskite at ~23 GPa
234 and 1873K were 0.6-0.8 wt% and less than 0.1 wt%, respectively. Because the H₂O
235 content in perovskite was quite small, the resulting calculated partition coefficient
236 between ringwoodite and perovskite exhibits larger scatter. Nevertheless, the results
237 show that the partition coefficient between ringwoodite and perovskite
238 ($K_d = (H_2O)_\gamma / (H_2O)_{Pv}$) could be determined to be ~15 in average; this result shows that
239 ringwoodite favors H₂O 15 times more compared with perovskite.

240 We have already determined that the partition coefficient between olivine and
241 wadsleyite ($K_d = (H_2O)_\beta / (H_2O)_\alpha$) was ~5 (Chen et al., 2002). Combining our previous
242 data with our present data, the partitioning of H₂O in olivine(α), wadsleyite(β),
243 ringwoodite(γ) and perovskite(Pv) could be determined as $\alpha : \beta : \gamma : Pv = 6 : 30 : 15 : 1$.
244 Olivine is the most abundant minerals in the mantle, so the H₂O partitioning among the
245 upper mantle, between 410-520 km and 520-660 km of the mantle transition zone, and
246 the lower mantle can be estimated as 6:30:15:1, respectively.

247 Because the maximum H₂O solubility in wadsleyite is 3.3 wt% (e.g. Inoue et al,
248 1995), the possible maximum H₂O storage capacities in the olivine high pressure
249 polymorphs are as follows; ~0.7 wt% in olivine (upper mantle just above 410 km
250 depth), ~3.3 wt% in wadsleyite (410-520 km depth), ~1.7 wt% in ringwoodite (520-660
251 km depth) and ~0.1 wt% in perovskite (lower mantle). With this consideration, we
252 adopted the maximum H₂O solubility in wadsleyite to discuss the maximum H₂O
253 storage capacity in the mantle. However, it was reported that the H₂O solubility
254 becomes lower with increasing temperature (e.g. Demouchy et al. 2005). The
255 temperature in the mantle transition zone is important to estimate the H₂O content.

256 In spite of the effect of temperature, the mantle transition zone should be a large
257 geochemical reservoir of water in the Earth's interior, and the maximum water storage
258 capacity in the mantle transition zone is ~4 times relative to the amount of sea water.
259 Note that the H₂O content in olivine was determined at ~13.5 GPa (just above 410 km
260 depth), and we know that the H₂O solubility in olivine increases with increasing
261 pressure as shown in Kohlstedt et al. (1996) and Hauri et al. (2006). In the shallower
262 mantle below 410 km depth, the H₂O content in olivine should become less with

263 decreasing pressure.

264

265 **3-4. Geophysical implication**

266 Knowledge of absolute water contents in the mantle is important because hydration
267 affects various physical properties of mantle minerals (e.g. Inoue et al, 1998; Jacobsen
268 et al., 2004; Huang et al., 2005). Therefore, many researchers have made an effort to
269 estimate the absolute water content in the mantle. Especially, seismological and
270 electrical conductivity observations combined with laboratory measured values enable
271 us to estimate the water content in the mantle. Mantle transition zone minerals,
272 wadsleyite and ringwoodite, can accommodate significant amount of H₂O (up to 2-3
273 wt%) in their crystal structures, so these minerals should be key minerals to contain
274 water in the mantle.

275 Suetsugu et al. (2006) and Yamada et al. (2009) tried to estimate temperature
276 anomalies and water content in the mantle transition zone just above the 660 km
277 discontinuity beneath the Japan Islands and the Philippine Sea from tomographically
278 determined P-velocity anomalies and the depth of the 660-km discontinuity determined
279 by the receiver function method. The water content beneath the Philippine Sea and
280 western Japan, where the Pacific slab is subducted, was estimated to be in the range of
281 1-1.5 wt% H₂O, and the west Philippine basin, away from the Pacific slab, did not have
282 any significant water content. This estimated H₂O content shows the relative water
283 content anomaly with respect to average values in their study regions, because
284 tomographically determined P-velocity anomalies were used as mentioned in Yamada et
285 al. (2009). They observed the apparently unreasonable negative values of water content
286 (-0.5 wt%) beneath northern Japan, and interpreted that the average H₂O content could
287 be regarded as ~0.5 wt% in the region, when it is regarded as a situation of absolutely
288 null water (dry). Recently, Suetsugu et al. (this issue) applied the same method by
289 using a new data set of ocean bottom geophysical observations beneath the Philippine
290 Sea and the northwestern Pacific Ocean, and revised the water content and estimated
291 that there was less than 0.2 wt% H₂O beneath these areas. Although they mentioned that
292 the estimated water content had an uncertainty of about 0.2-0.3 wt% H₂O, the average
293 H₂O content in these areas was considered to be ~0.1 wt% H₂O from Figure 7 in
294 Suetsugu et al. (this issue). Note that this estimated H₂O contents reflects that in
295 ringwoodite.

296 On the other hand, the electrical conductivities of wadsleyite and ringwoodite in
297 anhydrous and hydrous forms were measured (Huang et al., 2005; Yoshino et al., 2008;
298 Manthilake et al., 2009; Dai and Karato, 2009), and compared to the geophysical
299 observations to estimate the water content. Though there are some arguments about the
300 estimated water content (Karato and Dai, 2009; Yoshino and Katsura, 2009), their recent
301 conclusions show that some water (~0.1–0.3 wt% in the Pacific) is required to explain
302 the observed electrical conductivity (Dai and Karato, 2009). In addition, though Yoshino
303 et al. (this issue) mentioned that the present conductivity-depth profiles in the transition
304 zone agreed with that obtained from the geophysical observations beneath the Pacific in
305 the case of the mantle transition zone, 0.1-0.2 wt% H₂O explains the recent geophysical
306 reference model (Shimizu et al., submitted) from Figure 6 in Yoshino et al. (this issue).
307 Still more, Yoshino et al. (this issue) mentioned that the presence of water in the
308 transition zone minerals is required to explain the high conductivity beneath the
309 Philippine Sea and northeastern China (Baba et al., this issue).

310 In this study, we determined the partitioning of H₂O among olivine high pressure
311 polymorphs. When we apply ~0.2 wt% of the H₂O content in wadsleyite in the mantle
312 transition zone estimated by the recent electrical conductivity measurements (e.g. Dai
313 and Karato, 2009), the estimated H₂O content in the mantle is as follows; ~0.04 wt% in
314 olivine (upper mantle), ~0.2 wt% in wadsleyite (410-520 km depth), ~0.1 wt% in
315 ringwoodite (520-660 km depth), and ~0.007 wt% in perovskite (lower mantle). These
316 estimated values satisfy, within the error, the recently estimated H₂O content in mantle
317 transition zone minerals (i.e. wadsleyite and ringwoodite) by different methods based on
318 seismological and electrical conductivity observations.

319 Thus, the mantle transition zone should be a large geochemical reservoir of water in
320 the Earth's mantle compared with the upper and lower mantle. Additionally, the amount
321 of water in the mantle transition zone is ~0.3 times more relative to that of sea water,
322 when mantle wadsleyite contains ~0.2 wt% H₂O.

323

324 **4. Conclusions**

325 We have determined the water partitioning between wadsleyite and ringwoodite, and
326 ringwoodite and perovskite. The results are as follows; olivine : wadsleyite :
327 ringwoodite : perovskite = 6: 30: 15 : 1. In addition, the phase boundary of
328 olivine-wadsleyite, wadsleyite-ringwoodite, and postspinel transformations move to the

329 low, high, and high pressure side, respectively, with the effect of water, when we
330 combine the present data with our previous data (Higo et al., 2001; Chen et al., 2002;
331 Inoue et al., 2010). The resultant H₂O partitioning of $[H_2O]_{\alpha} < [H_2O]_{\beta} > [H_2O]_{\gamma} >$
332 $[H_2O]_{pv}$ is consistent with the results of the effect of water on the high pressure phase
333 boundary of olivine.

334 Because the maximum H₂O solubility in wadsleyite is 3.3 wt% (e.g. Inoue et al,
335 1995), the possible maximum H₂O storage capacity in the olivine high pressure
336 polymorphs are as follows; ~0.7 wt% in olivine (upper mantle just above 410 km depth),
337 ~3.3 wt% in wadsleyite (410-520 km depth), ~1.7 wt% in ringwoodite (520-660 km
338 depth), and ~0.1 wt% in perovskite (lower mantle).

339 When we apply ~0.2 wt% of the H₂O content in wadsleyite in the mantle transition
340 zone, the estimated H₂O content through the mantle are as follows; ~0.04 wt% in
341 olivine (upper mantle just above 410 km depth), ~0.2 wt% in wadsleyite (410-520 km
342 depth), ~0.1 wt% in ringwoodite (520-660 km depth), and ~0.007 wt% in perovskite
343 (lower mantle).

344 Thus, the mantle transition zone should contain a large water reservoir in the Earth's
345 mantle when compared to the upper and lower mantle. Additionally, if mantle
346 wadsleyite contains ~0.2 wt% H₂O then the mantle transition zone would contain
347 approximately one-third the H₂O mass of Earth's oceans.

348

349 **Acknowledgements**

350 We thank the constructive comments of two reviewers Dr. M. Akaogi and Dr. S.D.
351 Jacobsen to improve the manuscript. We also thank Sabrina Whitaker at the GRC,
352 Ehime University for the English improvement. This work was supported by a
353 Grant-in-Aid for Scientific Research (A) [KAKENHI] from Japan Society for the
354 Promotion of Science (JSPS) given to Toru Inoue, and a Global COE program from the
355 Ministry of Education, Culture, Sports, Science and Technology (MEXT).

356

357 **References**

358 Akaogi, M., Ito, E., Novrotzky, A., 1989. Olivine-modified spinel-spinel transitions in
359 the system Mg₂SiO₄-Fe₂SiO₄: Calorimetric measurements, thermochemical
360 calculation, and geophysical application, J. Geophys. Res., 94, 15671-15685.

361 Baba, K., Utada, H., Goto, T., Kasaya, T., Shimizu, H., Tada, N., Electrical conductivity
362 imaging of the Philippine Sea upper mantle using seafloor magnetotelluric data.
363 Phys. Earth Planet. Inter. (this issue)

364 Bolfan-Casanova, N., H. Keppler, Rubie, D.C., 2003. Water partitioning at 660 km
365 depth and evidence for very low water solubility in magnesium silicate perovskite,
366 Geophys. Res. Lett., 30, 1905, doi: 10.1029/2003GL017182.

367 Brown, J.M. and Shankland, T.J., 1981. Thermodynamic parameters in the Earth as
368 determined from seismic profiles. Geophys. J., Royal Astronomical Society, 66(3),
369 579-596.

370 Chen, J., Inoue, T., Yurimoto, H., Weidner, D.J., 2002. Effect of water on
371 olivine-wadsleyite phase boundary in the (Mg, Fe)₂SiO₄ system, Geophys. Res. Lett.,
372 29, 1875, doi:10.1029/2001GL014429.

373 Dai, L., Karato, S. 2009. Electrical conductivity of wadsleyite at high temperatures and
374 high pressures. Earth Planet. Sci. Lett., in press.

375 Demouchy, S., Deloule, D., Frost, D.J., Keppler, H., 2005. Pressure and temperature
376 dependence of water solubility in Fe-free wadsleyite. Am. Mineral., 90,
377 1084-1091.

378 Frost, D. J., Dolejs, D, 2007. Experimental determination of the effect of H₂O on the
379 410-km seismic discontinuity. Earth Planet. Sci. Lett., 256, 182-195.

380 Hauri, E.H., Gaetani, G.A., Green, T.H., 2006. Partitioning of water during melting of
381 the Earth's upper mantle at H₂O-undersaturated conditions. Earth Planet. Sci. Lett.,
382 248, 715-734.

383 Higo, Y., Inoue, T., Irifune T., Yurimoto, H., 2001. Effect of water on the
384 spinel-postspinel transformation in Mg₂SiO₄. Geophys. Res. Lett., 28, 3505-3508.

385 Huang, X., Xu, Y., Karato, S., 2005. Water content in the transition zone from electrical
386 conductivity of wadsleyite and ringwoodite. Nature, 434, 746-749.

387 Inoue, T., 1994. Effect of water on melting phase relations and melt composition in the
388 system Mg₂SiO₄-MgSiO₃-H₂O up to 15 GPa. Phys. Earth Planet. Inter., 85,
389 237-263.

390 Inoue, T., Yurimoto H., Kudoh, Y., 1995. Hydrous modified spinel, Mg_{1.75}SiH_{0.5}O₄: a
391 new water reservoir in the mantle transition region, Geophys. Res. Lett., 22,
392 117-120.

- 393 Inoue, T., Weidner, D.J., Northrup P.A., Parise, J.B., 1998. Elastic properties of hydrous
394 ringwoodite (γ -phase) on Mg_2SiO_4 , *Earth Planet. Sci. Lett.*, 160, 107-113.
- 395 Inoue, T. Ueda, T., Tanimoto, Y., Yamada, A., Irifune, T., 2010. The effect of water on
396 the high-pressure phase boundaries in the system Mg_2SiO_4 - Fe_2SiO_4 . *J. Phys.: Conf.*
397 *Ser.*, 215, 012101.
- 398 Jacobsen, S.D., Smyth, J.R., Spetzler, H., Holl, C.M., Frost, D.J., 2004. Sound
399 velocities and elastic constants of iron-bearing hydrous ringwoodite. *Phys. Earth*
400 *Planet. Inter.*, 143-144, 47-56.
- 401 Irifune, T., Kubo, N., Isshiki, M., Yamazaki, Y., 1998. Phase transformations in
402 serpentine and transportation of water into the lower mantle. *Geophys. Res. Lett.*,
403 25, 203-206.
- 404 Ito, E., Takahashi, E., 1989. Postspinel transformations in the system Mg_2SiO_4 - Fe_2SiO_4
405 and some geophysical implications, *J. Geophys. Res.*, 94, 10,637-10,646.
- 406 Karato, S., Dai, L., 2009. Comments on “Electrical conductivity of wadsleyite as a
407 function of temperature and water content” by Manthilake et al., *Phys. Earth Planet.*
408 *Inter.*, 174, 19-21.
- 409 Katsura, T., Shatskiy, A., Manthilake, M.A.G.M., Zhai, S., Fukui, H., Yamazaki, D.,
410 Matsuzaki, T., Yoneda, A., Ito, E., Kuwata, A., Ueda, A., Nozawa, A., Funakoshi,
411 K., 2009. Thermal expansion of forsterite at high pressures determined by in situ
412 X-ray diffraction: The adiabatic geotherm in the upper mantle. *Phys. Earth Planet.*
413 *Inter.*, 174, 86-92.
- 414 Kohlstedt, D.L., Keppler, H., Rubie, D.C., 1996. Solubility of water in the α , β and γ
415 phases of $(Mg,Fe)_2SiO_4$. *Contrib. Mineral. Petrol.*, 123, 345-357.
- 416 Kurosawa, M., Yurimoto, H., Sueno, S., 1997. Patterns in the hydrogen and trace
417 element compositions of mantle olivines. *Phys. Chem. Minerals*, 24, 385-395.
- 418 Manthilake, M.A.G.M., Matsuzaki, T., Yoshino, T., Yamashita, S., Ito, E., Katsura, T.,
419 2009. Electrical conductivity of wadsleyite as a function of temperature and water
420 content. *Phys. Earth Planet. Inter.*, 174, 10-18.
- 421 Mibe, K. Kanzaki, M., Kawamoto, T., Matsukage, K.N., Fei, Y., Ono, S., 2007. Second
422 critical end point in the peridotite-H₂O system. *J. Geophys. Res.*, 112, B03201.
- 423 Miyagi, I., Yurimoto, H., 1995. Water content of melt inclusions in phenocrysts using
424 secondary ion mass spectrometer. *Bull. Volcanol. Soc. Jpn.*, 40, 349-355.

425 Miyagi, I. Matsubaya, O., Nakashima, S., 1998. Change in D/H ratio, water content and
426 color during dehydration of hornblende. *Geochem. J.*, 32, 33-48.

427 Ohtani, E., Litasov, K., Hosoya, T., Kubo, T., Kondo, T., 2004. Water transport into
428 deep mantle and formation of a hydrous transition zone, *Phys. Earth Planet. Inter.*,
429 143-144, 255-269.

430 Shimizu, H. Koyama, T., Baba, H., Utada, H. Revised 1-D mantle electrical
431 conductivity structure beneath the north Pacific. *Geophys. Int. J.* (submitted)

432 Suetsugu, D., Inoue, T. Yamada, A., Zhao, D., Obayashi, M., 2006. Towards mapping
433 the three-dimensional distribution of water in the transition zone from P-velocity
434 tomography and 660-km discontinuity depths. In "Earth's deep water cycle,
435 Geophysical monograph series 168", Ed. by Steven D. Jacobsen and Suzan van
436 der Lee, AGU, pp.237-249.

437 Suetsugu, D., Inoue, T., Obayashi, M., Yamada, A., Shiobara, H., Sugioka, H., Ito, A.,
438 Kanazawa, T., Kawakatsu, H., Shito, A., Fukao, Y. Depths of the 410-km and
439 660-km discontinuities in and around the stagnant slab beneath the Philippine Sea:
440 Is water stored in the stagnant slab? *Phys. Earth Planet. Inter.* (this issue)

441 Yamada, A., Inoue, T., Irifune, T., 2004. Melting of enstatite from 13 to 18 GPa under
442 hydrous conditions, *Phys. Earth Planet. Inter.*, 147, 45-56.

443 Yamada, A., Zhao, D., Inoue, T., Suetsugu, D., Obayashi, M., 2009. Seismological
444 evidence for compositional variations at the base of the mantle transition zone
445 under Japan Islands, *Gondwana Research* , 16, 482-490.

446 Yoshino, T., Manthilake, G., Matsuzaki, T., Katsura, T., 2008. Dry mantle transition
447 zone inferred from electrical conductivity of wadsleyite and ringwoodite. *Nature*
448 451, 326-329.

449 Yoshino, T., Katsura, T., 2009. Reply to Comments on "Electrical conductivity of
450 wadsleyite as a function of temperature and water content" by Manthilake et al.,
451 *Phys. Earth Planet. Inter.*, 174, 22-23.

452 Yoshino, T., Katsura, T., Baba, K., Utada, H. Laboratory-based conductivity structure in
453 the mantle transition zone. *Phys. Earth Planet. Inter.* (this issue)

454 Yurimoto, H., Kurosawa, M., Sueno, S. 1989. Hydrogen analysis in quartz crystals and
455 quartz glass by secondary ion mass spectrometry. *Geochim. Cosmochim. Acta* 53,
456 751-755.

457

458

459

460 **Figure captions**

461

462 Figure 1. An example of the cell assembly used in the present experiments for the
463 wadsleyite-ringwoodite transformation.

464

465 Figure 2. (a) High pressure phase diagram of olivine high pressure polymorphs under
466 anhydrous condition at T=1673K. The solid line represents the phase boundary from
467 Akaogi et al. (1989) under anhydrous condition. Using this plot, the run pressures were
468 determined.

469 (b) High pressure phase diagram of olivine high pressure polymorphs under hydrous
470 condition at T=1673K. The broken line represents the phase boundary from Akaogi et al.
471 (1989) under anhydrous condition, and the solid line represents that under hydrous
472 condition from Inoue et al. (2010). The present results are consistent with our previous
473 boundary of Inoue et al. (2010).

474 Open triangles and squares show the assemblages of the single wadsleyite phase and
475 that of the single ringwoodite phase, respectively, and filled triangles and squares show
476 the wadsleyite coexisting with ringwoodite, and the ringwoodite coexisting with
477 wadsleyite, respectively. α : olivine, β : wadsleyite, γ : ringwoodite.

478

479 Figure 3. Back scattered electron image of run products (a) E1751 and (b) E1760. β :
480 wadsleyite, γ : ringwoodite, CEn: clinoenstatite, L: liquid.

481

482 Figure 4. Back scattered electron image of run products (a) E1784 and (b) E1730. γ :
483 ringwoodite, Pv: perovskite, L: liquid.

484

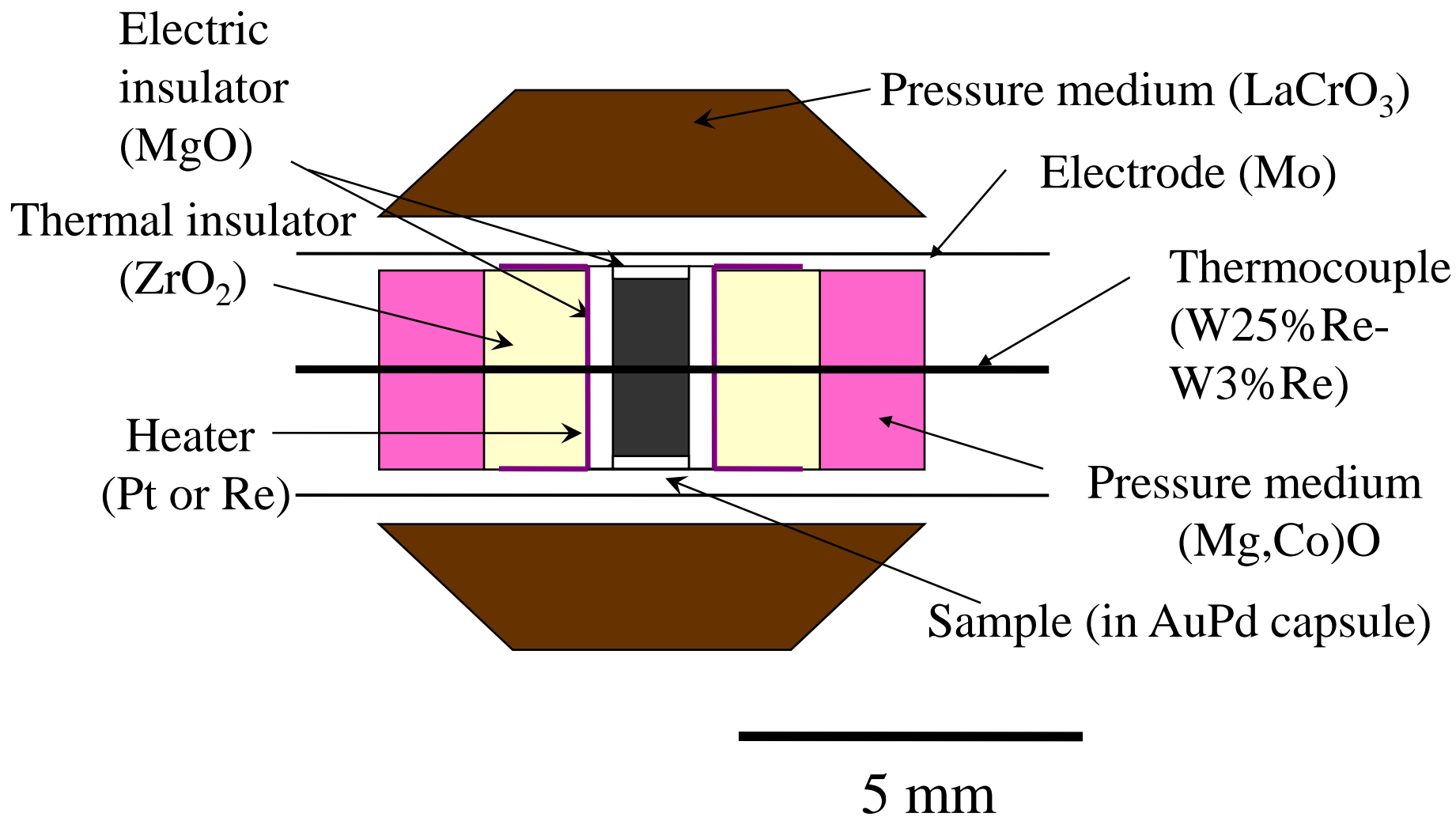


Fig. 1 Inoue et al.

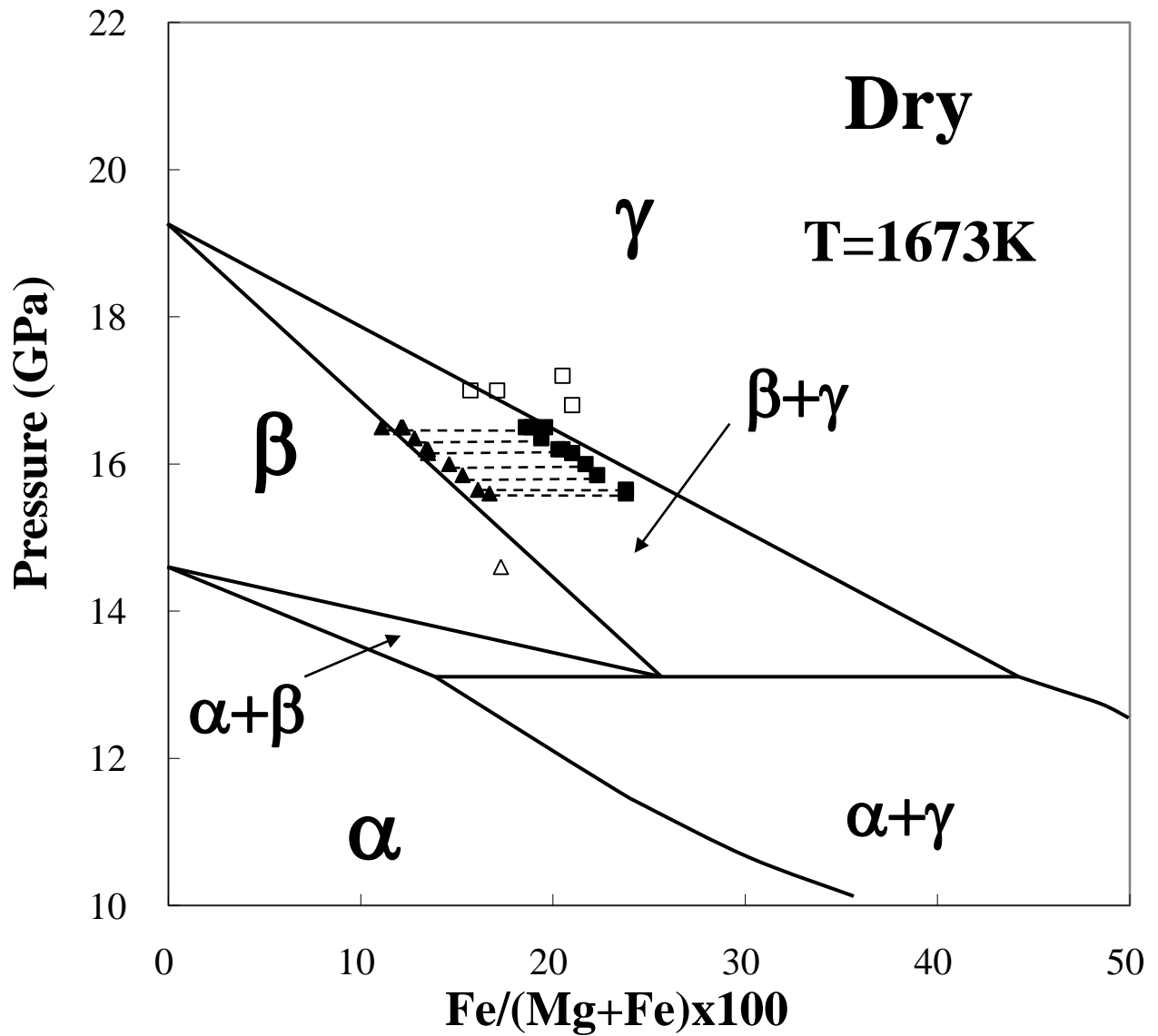


Fig. 2 (a) Inoue et al.

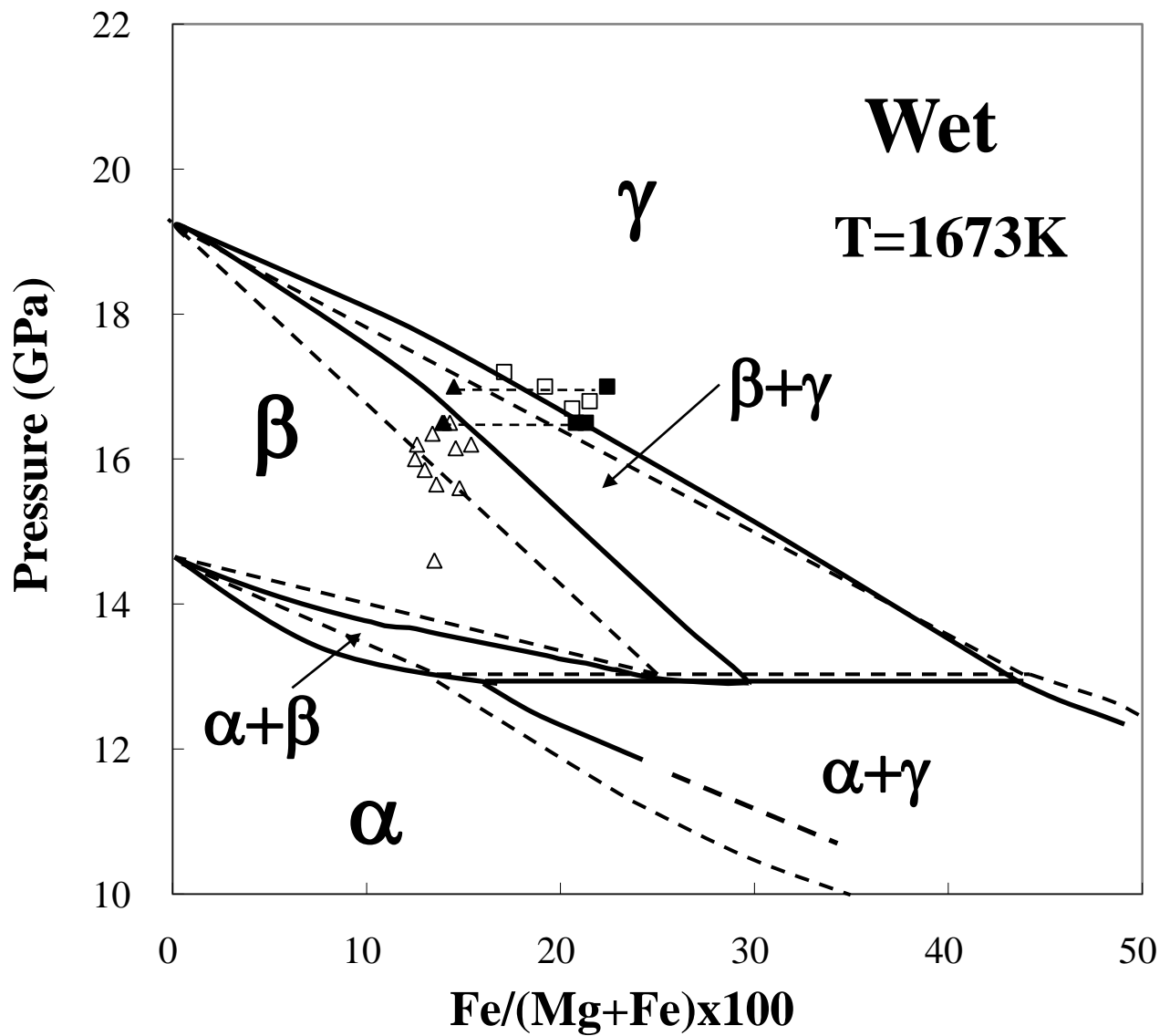
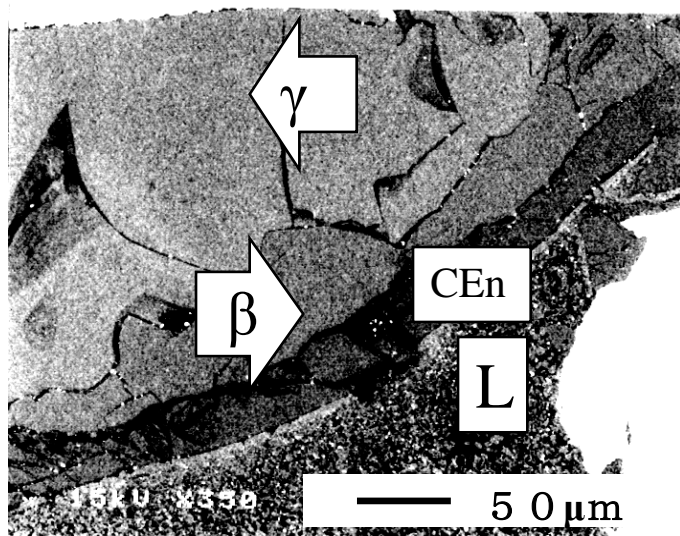


Fig. 2 (b) Inoue et al.

(a) E1751 WET
16.5GPa, 1673K



(b) E1760 WET
16.5GPa, 1673K

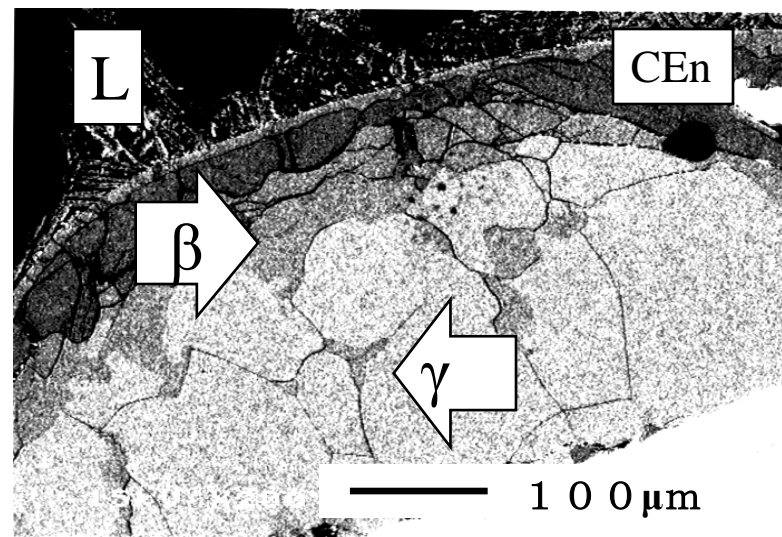
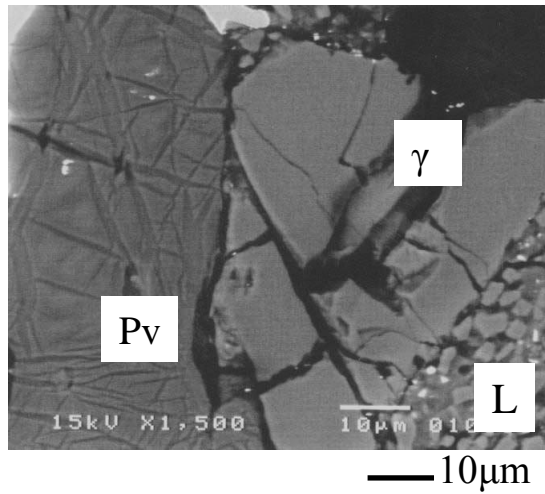


Fig. 3 Inoue et al.

(a) E1784 WET
23.0GPa, 1873K



(b) E1730 WET
23.1GPa, 1873K

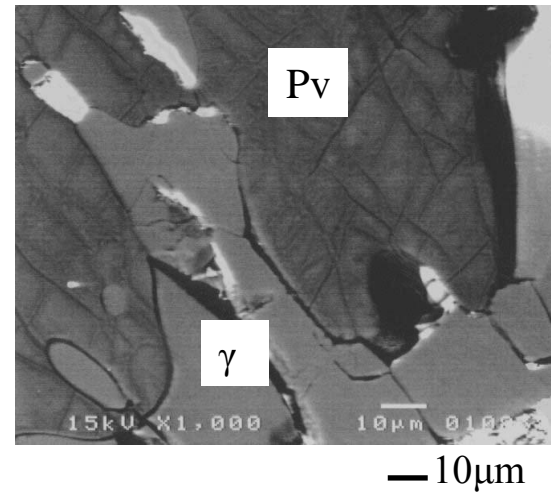


Fig. 4 Inoue et al.

Table 1. Chemical composition of starting material

	Dry	Wet
MgO	42.1	35.4
FeO	18.7	15.8
SiO ₂	39.2	33.0
H ₂ O	-	15.8
Total (wt%)	100.0	100.0
(Mg+Fe)/Si	2.0	2.0
Fe/(Mg+Fe)	0.2	0.2

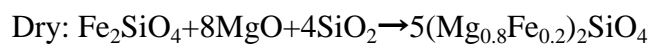


Table 2. Experimental conditions and the results (T=1673K)

Run No.	Load (ton)	Pressure (GPa)	Time (min)	Dry	Wet
E1672	412	14.6	60	β	$\beta+L$
E1766	480	15.6	120	$\beta+\gamma$	$\beta+CEn+L$
E1748	470	15.7	60	$\beta+\gamma$	$\beta+CEn+L$
E1678	500	15.9	60	$\beta+\gamma$	$\beta+CEn+L$
E1789	490	16.0	60	$\beta+\gamma$	$\beta+L$
E1786	483	16.2	90	$\beta+\gamma$	$\beta+CEn+L$
E1805	506	16.2	90	$\beta+\gamma$	$\beta+CEn+L$
E1744	505	16.2	60	$\beta+\gamma$	$\beta+CEn+L$
E1807	506	16.4	90	$\beta+\gamma$	$\beta+CEn+L$
E1794	500	16.5	90	$\beta+\gamma$	$\beta+L$
E1760	485	16.5	90	$\beta+\gamma$	$\beta+\gamma+CEn+L$
E1751	510	16.5	120	$\beta+\gamma$	$\beta+\gamma+CEn+L$
E1788 [*]	485	~17#	60	γ	$\beta+\gamma+CEn+L$
E1758	508	~17#	60	γ	$\gamma+St+L$
E1738 [*]	520	16.7	60	γ	$\gamma+L$
E1731	525	16.8	60	γ	$\gamma+L$
E1683	550	17.2	60	γ	$\gamma+L$

β : wadsleyite, γ : ringwoodite, CEn: clinoenstatite, St: stishovite, L: liquid

* Temperatures were estimated by power supply.

These pressure should have large uncertainty.

Table 3. Experimental conditions and the results (T=1873K)

Run No.	Load (ton)	Pressure (GPa)	Time (min)	Dry	Wet
E1720	435	22.9	60	γ	Pv + L
E1767	435	22.9	120	$\gamma\#$	SuB+D+Mw+L
E1749*	440	23.0	120	$\gamma\#$	Pv + L
E1759*	440	23.0	120	$\gamma\#$	Pv+Mw+SuB+L
E1770	440	23.0	120	Pv + Mw	Pv + Mw + L
E1784*	440	23.0	20	γ + Pv + Mw	γ + Pv + L
E1730	445	23.1	60	γ + Pv + Mw	γ + Pv + L
E1787	445	23.1	60	γ	Pv + L
E1688	450	23.2	60	γ + Pv + Mw	Pv + L
E1695	450	23.2	30	γ + Pv + Mw	γ + Pv + L
E1796	450	23.2	60	$\gamma\#$	γ +Mw+SuB+D+L

γ : ringwoodite, Pv: perovskite, Mw: magnesiowustite, St: stishovite

SuB: superhydrous phase B, D: phase D, L: liquid

*Temperatures were estimated by power supply.

#Small amounts of magnesiowustite and stishovite exist in the run charge.

Table 4. Fe/(Mg+Fe) in β and γ and the partitioning (T=1673K)

Run No.	Pressure (GPa)	Dry			Wet		
		Fe/(Mg+Fe)		Kd	Fe/(Mg+Fe)		Kd
		β	γ		β	γ	
E1672	14.6	0.173(6)	----		0.135(5)	----	
E1766	15.6	0.167(1)	0.238(4)	1.56	0.148(28)	----	
E1748	15.7	0.161(4)	0.238(11)	1.62	0.136(3)	----	
E1678	15.9	0.153(1)	0.223(2)	1.59	0.130(4)	----	
E1789	16.0	0.146(2)	0.217(2)	1.62	0.125(1)	----	
E1786	16.2	0.135(7)	0.210(6)	1.71	0.146(3)	----	
E1805	16.2	0.134(6)	0.205(5)	1.67	0.154(7)	----	
E1744	16.2	0.135(1)	0.203(6)	1.64	0.126(5)	----	
E1807	16.4	0.128(3)	0.194(2)	1.65	0.134(2)	----	
E1794	16.5	0.122(1)	0.186(5)	1.65	0.143(11)	----	
E1760	16.5	0.121(5)	0.189(6)	1.70	0.139(4)	0.213(8)	1.68
E1751	16.5	0.111(4)	0.196(3)	1.95	0.140(5)	0.208(3)	1.62
E1788*	~17#	----	0.157(6)		0.145(3)	0.224(3)	1.70
E1758	~17#	----	0.171(5)		----	0.192(6)	
E1738*	16.7		N.A.		----	0.206(4)	
E1731	16.8	----	0.210(2)		----	0.215(2)	
E1683	17.2	----	0.205(2)		----	0.171(14)	

(): standard deviation; N.A. not analyzed; * Temperatures were estimated by power supply.

Kd = $(\text{Fe}/\text{Mg})_{\gamma} / (\text{Fe}/\text{Mg})_{\beta}$; # These pressure should have large uncertainty.

Table 5. Fe/(Mg+Fe) in γ and perovskite and the partitioning (T=1873K)

Run No.	Pressure (GPa)	Dry				Wet	
		Fe/(Mg+Fe)				Fe/(Mg+Fe)	
		γ	Pv	Mw	Kd	γ	Pv
E1784*	23.0	0.199(9)	0.086(1)	0.342(2)	0.38	0.159(1)	0.056(3)
E1730	23.1	0.188(1)	N.A.	N.A.		0.135(2)	0.063(4)
E1695	23.2	0.178(4)	0.084(6)	N.A.	0.42	0.087(2)	0.049(3)

(): standard deviation; N.A. not analyzed; * Temperatures were estimated by power supply.

$$Kd = (Fe/Mg)_{Pv} / (Fe/Mg)_{\gamma}$$

Table 6. H₂O partitioning between wadsleyite (β) and ringwoodite (γ)
 T=1673K

Run No.	Pressure (GPa)	H ₂ O wt%		Kd
		β	γ	
E1788*-1	~17	3.72	1.69	2.2
E1760-1	16.5	2.28	1.11	2.05
E1760-2	16.5	2.24	1.25	1.79
E1751-1	16.5	1.88	1	1.88
E1751-2	16.5	1.79	1.1	1.63
average				1.9(2)

* Temperature was estimated by power supply.

(): standard deviation, $Kd=(H_2O)_\beta/(H_2O)_\gamma$

Table 7. H₂O partitioning between ringwoodite (γ) and perovskite (Pv)

T=1873K

Run No.	Pressure (GPa)	H ₂ O wt%		Kd
		γ	Pv	
E1784*	23	0.76	0.06	13
E1730	23.1	0.71(25)	0.03	24(8)
E1695	23.2	0.63(11)	0.07(3)	9(5)
average				15(8)

* Temperature was estimated by power supply.

(): standard deviation, $Kd=(H_2O)_{\gamma}/(H_2O)_{Pv}$